

# Power Management of Wireless In-Wheel Motor with Dynamic Wireless Power Transfer

Takuma Takeuchi\*, Takehiro Imura\*, Hiroshi Fujimoto\*\*, Yoichi Hori\*\*\*

The University of Tokyo

5-1-5, Kashiwanoha, Kashiwa, Chiba, 227-8561, Japan

Phone: +81-4-7136-3873\*, +81-4-7136-4131\*\*, +81-4-7136-3846\*\*\*

Email: takeuchi@hflab.k.u-tokyo.ac.jp,

imura@hori.k.u-tokyo.ac.jp,

fujimoto@k.u-tokyo.ac.jp,

hori@k.u-tokyo.ac.jp

**Abstract**—In-Wheel Motor (IWM) which is a driving system of Electric Vehicles (EVs) is effective for improving driving stability of vehicle and reducing vehicle weight. However, IWM has not been put in practical use because of a possibility of power lines disconnection. Therefore, we have proposed Wireless In-Wheel Motor (W-IWM) in which Wireless Power Transfer (WPT) is used to remove these lines and to enhance practicability of IWM. Moreover, we have proposed the advanced system of W-IWM which has Lithium-ion Capacitor (LiC) and circuit for Dynamic Wireless Power Transfer (DWPT) on its wheel-side. In this paper, power management on the wheel-side is proposed. By applying this control method, efficiency of regenerative breaking can be improved. Moreover, dynamic wireless power transfer from road-side infrastructure can be achieved on the wheel-side. The proposed method is verified by simulations and experiments.

**Index Terms**—Wireless In-Wheel Motor, Wireless Power Transfer, Lithium-ion Capacitor, Power management, State of Charge, Dynamic Wireless Power Transfer

## I. INTRODUCTION

Electric Vehicles (EVs) have been gathering a great deal of public attention from the perspective of environmental performance. However, due to a limited battery capacity, EVs has been only able for short distance. To deal with this problem, a number of researches have been done on effective motor driving for EVs [1] or driving range extension by vehicle motion control using In-Wheel Motor (IWM) [2], [3]. IWM is one of the drive systems which equipped motors in its wheels. Owing to the independent torque control of each wheel, IWM can achieve high vehicle stability and long driving range [4]. Nevertheless, IWM has not been put to practical use due to the risk of power lines disconnection mainly caused by continuous displacement between wheels and chassis while driving.

Therefore, we have proposed Wireless In-Wheel Motor (W-IWM) to solve this problem radically and to make IWM more practical by using Wireless Power Transfer (WPT) via magnetic resonance coupling [5], [6], [7]. We have already succeeded in driving an experimental vehicle with the first trial unit of W-IWM. The first trial unit of W-IWM achieves 3.3 kW/wheel and 89 % DC to DC efficiency from the chassis-side



(a) The first trial unit of W-IWM (b) Experimental vehicle

Fig. 1. The first trial unit of W-IWM and experimental vehicle.

to the wheel-side [8]. For more improvement of practicability, high power and further effective operation are expected.

Accordingly, the second trial unit of W-IWM (W-IWM2), which has Lithium-ion Capacitor (LiC) on the wheel-side for high output and a more efficient operation is under construction. W-IWM2 enables more efficient regenerative breaking from wheel power to LiC because the regenerative power goes through less number of converters. Additionally, circuit for Dynamic Wireless Power Transfer (DWPT) from a road-side facility is also added on wheel-side for more range extension.

As a result, W-IWM2 has multiple power sources [9], [10] on the wheel-side. Therefore, power-flow control of these power sources is required for stable motor driving. When too much/insufficient power are supplied from these power sources, the wheel-side DC-link voltage goes up/down. Moreover, regenerative power should goes through LiC for efficiency improvement. Therefore, power management on the wheel-side is necessary for W-IWM2.

In this paper, we propose power management method on the wheel-side by State of Charge (SOC) control of LiC. Applying this control to W-IWM2, a voltage of LiC is stabilized and output/input power of LiC can be controlled properly according to a load fluctuation. The proposed power management method is verified by simulations and experiments.

## II. WIRELESS IN-WHEEL MOTOR2 (W-IWM2)

Fig. 1 shows the first trial unit and the experimental vehicle. Fig. 2 shows a system configuration of W-IWM. By applying a hysteresis control to the wheel-side AC/DC converter, this

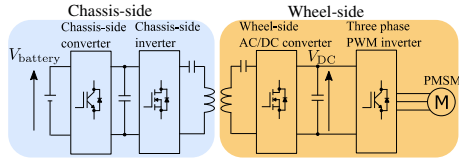


Fig. 2. System configuration of W-IWM.

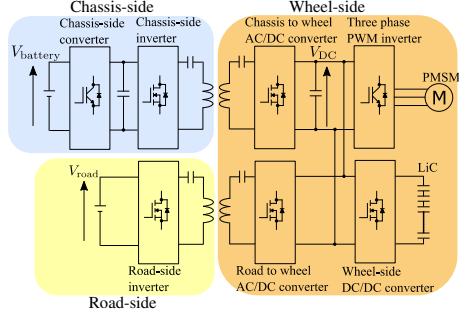


Fig. 3. System configuration of W-IWM2.

system stabilizes wheel-side DC-link voltage  $V_{DC}$  and controls receiving power via WPT simultaneously [8]. On the other hand, Fig. 3 shows a system of W-IWM2. In this system, LiC is connected to the DC-link through a wheel-side DC/DC converter, and a coil for DWPT from the road-side is also connected to the DC-link through an AC/DC converter.

Whereas W-IWM regenerates wheel power to the chasis-side via WPT, W-IWM2 can regenerate wheel power to LiC via the wheel-side DC/DC converter. Therefore, regenerative power goes through a small number of converters compared to W-IWM. DC to DC efficiency is expected to be improved from 89 % to 96 %. Additionally, DWPT from the road can be applied to W-IWM2. Thus more range extension can be expected.

### III. POWER MANAGEMENT ON THE WHEEL-SIDE

This chapter describes the proposed power management on the wheel-side.

#### A. wheel-side DC/DC converter

The wheel-side DC/DC converter controls the wheel-side DC-link voltage  $V_{DC}$ . By means of this voltage feedback control, a variation of  $V_{DC}$  caused by a power-flow transition is suppressed and LiC power  $P_{LiC}$  compensates the power-flow. Since LiC power  $P_{LiC}$  is controlled automatically, the wheel-side power-flow control is achieved only by the DC-link voltage  $V_{DC}$  feedback control.

#### B. wheel-side AC/DC converter

The wheel-side AC/DC converter controls the receiving power from the chasis-side via WPT  $P_{WPT}$ . By means of  $P_{WPT}$  control of the wheel-side AC/DC converter,  $P_{LiC}$  which is controlled by  $V_{DC}$  feedback control can be controlled indirectly.

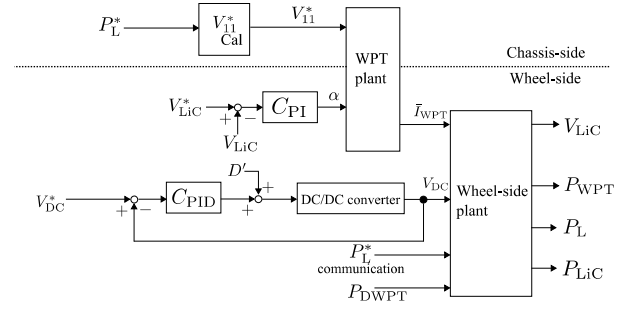


Fig. 4. Block diagram of W-IWM2.

With this  $P_{WPT}$  control, we can control SOC of LiC. In the case of a sudden acceleration where SOC of LiC decreases,  $P_{WPT}$  increases to compensate SOC. In contrast, in the case of a deceleration where SOC of LiC increases,  $P_{WPT}$  decreases to compensate SOC. Hereby the wheel-side power management can be achieved.

By the combination of these two controls, a relational expression on the power-flow of the wheel-side is fulfilled as follows:

$$P_L = P_{WPT} + P_{LiC} + P_{DWPT}, \quad (1)$$

where  $P_L$  is load power of PMSM and three phase PWM inverter.  $P_{LiC}$  is controlled by SOC control of LiC indirectly. Therefore the power management can be achieved. In addition, DWPT from the road-side can be achieved with these controls because an intermittent transmitting power from the road-side  $P_{DWPT}$  is buffered by LiC [10] and the motor can be driven by DWPT stably. The block diagram of the proposed SOC control of LiC is shown in Fig. 4.

## IV. CONTROLLERS

In this section, modeling and controllers for converters are described.

#### A. Voltage feedback control on the wheel-side DC/DC converter

The wheel-side DC/DC converter controls the wheel-side DC-link voltage  $V_{DC}$ . Fig. 5 shows a circuit model of the wheel-side DC/DC converter, where  $V_{LiC}$  is voltage of LiC,  $r$  is equivalent series resistance of LiC and reactor,  $L$  is reactance of DC/DC converter,  $I_{LiC}$  is reactor current,  $I_{load}$  is load current, and  $C$  is capacitance of the wheel-side DC-link smoothing capacitor. In this model, PMSM and three phase PWM inverter are modeled by current source.

To analyze this circuit, the state-space averaging method is applied. In this paper, because switching of this half bridge is reciprocal, this model works in continuous current mode. Since the system includes nonlinearity, linearization on its equilibrium point and minute variations analysis are conducted. Subsequently, the transfer function  $\Delta P_v$  from  $\Delta d'(s)$

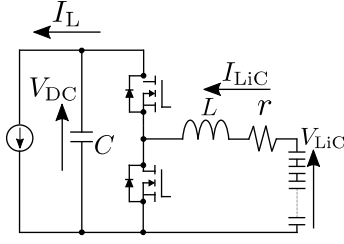


Fig. 5. Circuit model of wheel-side DC/DC converter.

to  $\Delta v_{DC}(s)$  is expressed as follows:

$$\begin{aligned} \Delta P_V &= \frac{\Delta v_{DC}(s)}{\Delta d'(s)} = \frac{b_{p1}s + b_{p0}}{s^2 + a_{p1}s + a_{p0}} \quad (2) \\ a_{p1} &= \frac{r}{L}, a_{p0} = -\frac{D'}{LC} \\ b_{p1} &= \frac{I_{LiC}}{C}, b_{p0} = \frac{rI_{LiC} - D'V_{DC}}{LC}, \end{aligned}$$

where  $\Delta d'(s)$  is a minute variation of the duty ration of the upper arm switch and  $\Delta v_{DC}(s)$  is a minute variation of the wheel-side DC-link voltage. Based on this transfer function, we design the PID controller such that closed-loop characteristic has quadrupole on real axis and discretized it with Tustin conversion.

### B. Power control on the wheel-side AC/DC converter

The wheel-side AC/DC converter controls the receiving power from the chassis-side to the wheel-side by two mode control [11]. Fig. 6 shows operation modes of the wheel-side AC/DC converter in two mode control.

#### Short mode

Low side switches of the wheel-side AC/DC converter are turn on. Then the wheel-side receiver coil shorts from the wheel-side circuit as shown in Fig. 6(a) and does not supply the transmitting power from the chassis-side to the wheel-side.

#### Rectification mode

The wheel-side AC/DC converter operates as a rectifier as shown in Fig. 6(b). The wheel-side receives the transmitting power from chassis to wheel.

By converting two modes periodically, we are able to control the average output current of the wheel-side AC/DC converter. Assuming that the wheel-side coil current is a sinusoidal current with the resonant frequency, an input voltage of the wheel-side AC/DC converter can be approached to its fundamental harmonic. Moreover, an approximate value of an effective current of the wheel-side coil  $I_{21}$  is determined as follow:

$$I_{21} \simeq \frac{\omega_0 L_m V_{11} - \frac{2\sqrt{2}}{\pi} R_1 V_{DC} \alpha}{R_1 R_2 + (\omega_0 L_m)^2}, \quad (3)$$

where  $\omega_0$  is resonance angular frequency,  $L_m$  is mutual inductance between the chassis-side and the wheel-side coils, and  $R_1, R_2$  are the chassis-side and the wheel-side coils

resistance respectively. An output current of the wheel-side AC/DC converter  $I_{WPT}$  on each mode is expressed as below.

$$I_{WPT} = \begin{cases} 0 & \text{(Short mode)} \\ \frac{2\sqrt{2}}{\pi} I_{21} & \text{(Rectification mode)} \end{cases} \quad (4)$$

Therefore, average output current of the wheel-side AC/DC converter  $\bar{I}_{WPT}$  is expressed with  $\alpha$ , which is time ration of rectification mode.

$$\bar{I}_{WPT} = \alpha I_{WPT} \quad (5)$$

Consequently, we can control an average output current of the wheel-side AC/DC converter  $\bar{I}_{WPT}$  and the receiving power from the chassis-side via WPT  $P_{WPT}$  by changing  $\alpha$ .

Generating a command value of this two mode control from  $V_{LiC}$  makes SOC control of LiC possible. Assuming that the  $V_{DC}$  control by the wheel-side DC/DC converter is valid, formula (6) is derived from formula (1) and the wheel-side circuit model can be expressed by Fig. 7.

$$I_{WPT} + I'_{LiC} = I_L \quad (6)$$

$I'_{LiC}$  is a output current of the wheel-side DC/DC converter. Assuming that a loss of the wheel-side DC/DC converter is small enough, formula (7) is derived.

$$I'_{LiC} V_{DC} = I_{LiC} V_{LiC} \quad (7)$$

Furthermore, a relation expression of a LiC current  $I_{LiC}$  and voltage  $V_{LiC}$  can be expressed as

$$I_{LiC} = -C_{LiC} \frac{dv_{LiC}}{dt}. \quad (8)$$

Therefore, from formula (6), (7) and (8), the following equation is derived.

$$\bar{i}_{WPT} = (C \frac{d}{dt} + \frac{1}{R_L}) v_{DC} + \frac{C_{LiC}}{v_{DC}} v_{LiC} \frac{dv_{LiC}}{dt} - i_{DWPT} \quad (9)$$

By linearizing the formula above using Taylor expansion, a transfer function from  $\Delta \bar{i}_{WPT}$  to  $\Delta v_{LiC}$  can be expressed as,

$$\Delta P_{SOC} = \frac{\Delta v_{LiC}}{\Delta \bar{i}_{WPT}} = \frac{V_{DC}}{2C_{LiC} V_{LiC} s}. \quad (10)$$

Consequently, we can design the PI controller for the circuit model expressed by formula (5) and (10) such that closed-lope poles have dual pole  $p_{PI}$  on real axis. Therefore, following PI gain are obtained.

$$K_P = \frac{\sqrt{2}\pi p_{PI} C_{LiC} V_{LiC} \{R_1 R_2 + (\omega_0 L_m)^2\}}{\omega_0 L_m V_{11} V_{DC}} \quad (11)$$

$$K_I = \frac{\pi p_{PI}^2 C_{LiC} V_{LiC} \{R_1 R_2 + (\omega_0 L_m)^2\}}{\sqrt{2}\omega_0 L_m V_{11} V_{DC}} \quad (12)$$

Finally, this PI controller is discretized with Tustin conversion.

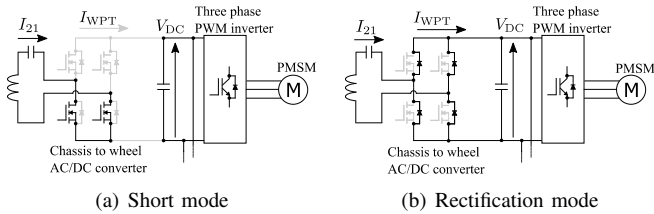


Fig. 6. Operation mode of 2mode control.

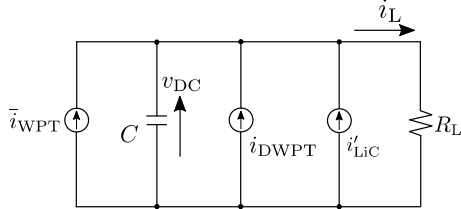


Fig. 7. Circuit model of the wheel-side on W-IWM2.

## V. SIMULATIONS

We performed simulations on the proposed SOC control of LiC using MATLAB Simulink Simpower Systems.

Simulation conditions are determined considering the value of W-IWM2 as given in Tab. I. The wheel-side DC-link voltage  $V_{DC}$  and an effective voltage of the chasis-side battery output  $V_1$  are determined by formula (13), (14) and (15) to make transmitting efficiency of WPT between the chasis-side and the wheel-side maximum and  $P_{WPT}$  8 kW during rectification mode.

$$R_{\eta opt} = \sqrt{\frac{R_2}{R_1}(\omega_0 L_m)^2 + R_2^2} \quad (13)$$

$$V_{DC} = \frac{\pi}{2\sqrt{2}} \sqrt{R_{\eta opt} P_{WPT}} \quad (14)$$

$$V_1 = \frac{R_1 R_2 + R_1 R_{\eta opt} + (\omega_0 L_m)^2}{(\omega_0 L_m)^2} V_{DC}, \quad (15)$$

where  $R_{\eta opt}$  is equivalent AC resistance of the wheel-side at the maximum efficiency of WPT ( $\alpha = 1$ ). Simulation steps are sampled at  $1.0 \times 10^{-7}$  sec. Moving average whose window size is 20000 is applied on power of simulation results to reduce effects of  $V_{DC}$  ripple and current ripple caused by two mode control on wheel-side AC/DC converter. We applied 1 kHz primary low pass filter on the load current  $i_L$ , the current of LiC  $i_{LiC}$ , and the output current of the wheel-side AC/DC converter  $\bar{I}_{WPT}$ .

### A. Load power fluctuation

We conducted a simulation on stepwise load power fluctuations. For simplicity, we excluded DWPT from the road-side in this simulation. Here, LiC powers/regenerates to compensate the wheel-side power-flow promptly. Therefore, SOC of LiC changes according to output/input power of LiC. Subsequently,  $P_{WPT}$  is controlled to make SOC of LiC follow the command value automatically.

Fig. 8 shows the simulation result in case of load power fluctuation. Fig. 8(a) shows power of each power source on

TABLE I  
SIMULATION AND EXPERIMENTAL PARAMETERS.

	Sim.	Exp.
Resonance frequency	85 kHz	85 kHz
Switching frequency of DC/DC converter	40 kHz	40 kHz
Switching frequency of 2mode control	500 Hz	500 Hz
chassis-side battery output voltage $V_1$	576.7 V	300.0 V
DC-link voltage reference $V_{DC}^*$	487.2 V	200.0 V
Maximum output	12.0 kW	1.2 kW
LiC capacitance	93.8 F	95.8F
LiC voltage reference $V_{LiC}^*$	48 V	50 V
chassis-side coil resistance $R_1$	400.0 m $\Omega$	558.09 m $\Omega$
chassis-side coil inductance $L_1$	270 $\mu$ H	269.63 $\mu$ H
wheel-side coil resistance $R_2$	300.0 m $\Omega$	361.81 m $\Omega$
wheel-side coil inductance $L_2$	250 $\mu$ H	224.51 $\mu$ H
Coil gap	100 mm	100 mm
Coil mutual inductance $L_m$	52.0 $\mu$ H	51.57 $\mu$ H
Smoothing capacitance $C$	2200 $\mu$ F	2145 $\mu$ F
Inductance of DC/DC converter $L$	60.8 $\mu$ H	60.8 $\mu$ H
ESR of inductance and LiC $r$	31.4 m $\Omega$	41.0 m $\Omega$

the wheel-side.  $P_{LiC}$  tracks stepwise changes of  $P_L$  rapidly, subsequently  $P_{WPT}$  is controlled to charge/discharge LiC automatically. Fig. 8(b) shows that the  $V_{DC}$  control of the wheel-side DC/DC converter can suppress  $V_{DC}$  variations caused by stepwise transitions of  $P_L$ . Fig. 8(c) shows that SOC of LiC tracks the command value before and after the load change.

Consequently, applying the proposed SOC control of LiC, the power management in the case of stepwise load fluctuations can be realized.

### B. Change of command value $V_{LiC}^*$

We conducted a simulation on command value changes of  $V_{LiC}^*$ . For simplicity, we excluded DWPT from the road-side in this simulation. Here,  $V^* LiC$  goes through a linear change from 48 V to 47 V. Subsequently,  $V_{LiC}^*$  changes linearly from 47 V to 48 V.

Fig. 9 shows the simulation result of command value changes of  $V_{LiC}^*$ . Fig. 9(a) shows power of each power source on the wheel-side.  $P_{WPT}$  changes to track a changing command value of  $V_{LiC}^*$  automatically. Fig. 9(c) shows voltage of LiC.  $V_{LiC}$  tracks a changing command value  $V_{LiC}^*$ . Therefore, we can confirm that SOC of LiC is stabilized by proposed SOC control.

Consequently, applying the proposed SOC control of LiC, the power management in the case of a changing command value of  $V_{LiC}^*$  can be realized.

### C. Power-flow change with Dynamic Wireless Power Transfer

We conducted a simulation on power-flow change with DWPT. When the load powers at 6.0 kW, the wheel-side receiving coil for DWPT moves at 80 km/h and receives transmitted power from the road-side.

Fig. 10(a) shows the experimental result of power-flow change with DWPT. Fig. 10(a) shows power of each power source on the wheel-side. While receiving DWPT from road-side, WPT from chasis-side stop automatically. Moreover, the load uses power of DWPT, then excess portion charge

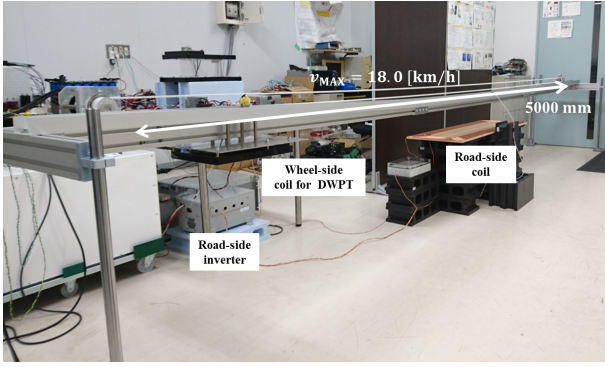


Fig. 12. Experimental setup for Dynamic Wireless Power Transfer.

LiC. Fig. 10(b) shows that the  $V_{DC}$  control of the wheel-side DC/DC converter can suppress  $V_{DC}$  variations caused by DWPT. Fig. 10(c) shows that SC is charged by DWPT and charged power is used by the load. Therefore we can confirm that the proposed SOC control is established.

Consequently, we verified that the power management in the case of receiving DWPT from road-side can be established by applying the proposed SOC control.

## VI. EXPERIMENTS

We conducted same experiments as simulations using the small power experimental setup shown in Fig. 11(a).

### A. Experimental setup

Fig. 11(b) shows a circuit diagram of a small power experimental setup. The bench test equipment is shown Fig. 12. This test bench can simulate driving motion of the wheel-side coil for DWPT. The wheel-side coil for DWPT moves toward the road-side coil at 18 km/h, and receives power transmitted from the road-side coil. To simplify the setup, a regenerative DC power supply (pCUBE MWBFP3-1250-J02 : Myway) replaces the PMSM and three phase PWM inverter. A DC power supply (PU300-5 : TEXIO) replaces battery and DC/DC converter on the chassis-side.

The experimental results are sampled at  $20 \times 10^{-6}$  sec. We filtered results of power by moving average with a window whose size is 2,000 to reduce  $V_{DC}$  and current ripple caused by two mode control of the wheel-side AC/DC converter. We applied 1 kHz primary low pass filter on the load current  $I_L$ , the current of LiC  $I_{LiC}$ , and the output current of the wheel-side AC/DC converter  $\bar{I}_{WPT}$ .

### B. Load power fluctuations

We conducted an experiment on stepwise load power fluctuations. Here we excluded DWPT from the road-side for simplicity.

Fig. ?? shows the experimental results of load power fluctuations. Fig. 13(a) shows power of each power source on the wheel-side. We can confirm that  $P_{LiC}$  tracks stepwise changes of  $P_L$  to compensate wheel-side power-flow rapidly. Subsequently,  $P_{WPT}$  changes to make voltage of LiC tracking a

command value  $V_{LiC}^*$  automatically. Because of the maximum transmitting power of the experimental setup is smaller than simulation, response of  $P_{WPT}$  is slower than the simulation result. Fig. 13(b) shows that the  $V_{DC}$  control of the wheel-side DC/DC converter can control  $V_{DC}$  changes caused by stepwise transitions of  $P_L$ . Fig. 13(c) shows that SOC of LiC tracks the command value before and after the load change.

Consequently, we verified that the power management in the case of stepwise load power fluctuations can be established by applying the proposed SOC control.

### C. LiC voltage command value $V_{LiC}$ change

We conducted an experiment on linear command value changes of  $V_{LiC}^*$ . For simplicity, we excluded DWPT from the road-side. Here  $V_{LiC}^*$  changed linearly from 50 V to 49 V. Subsequently,  $V_{LiC}$  changed linearly from 49 V to 50 V.

Fig. 14 shows the experimental result of command value changes of  $V_{LiC}^*$ . Fig. 14(a) shows power of each power source on the wheel-side. Because of the maximum transmitting power of the experimental setup is smaller than simulation, response of  $P_{WPT}$  is slower than the simulation result. Fig. 14(c) shows that  $V_{LiC}$  tracks the linear changing command value  $V_{LiC}^*$ . Therefore we can confirm that the proposed SOC control is established.

Consequently, we verified that the power management in the case of linear command value changes of  $V_{LiC}^*$  can be established by applying the proposed SOC control.

### D. Power-flow change with Dynamic Wireless Power Transfer

We conducted an experiment on power-flow change with DWPT. When the load powers at 1.0 kW, the wheel-side receiving coil for DWPT moves at 18 km/h and receives transmitted power from the road-side.

Fig. 15 shows the experimental result of power-flow change with DWPT. Fig. 15(a) shows power of each power source on the wheel-side. While receiving DWPT from road-side, WPT from chassis-side stop automatically. Moreover, the load uses power of DWPT, then excess portion charge SC. Fig. 15(b) shows that the  $V_{DC}$  control of the wheel-side DC/DC converter can suppress  $V_{DC}$  variations caused by DWPT. Fig. 15(c) shows that SC is charged by DWPT and charged power is used by the load. Therefore we can confirm that the proposed SOC control is established.

Consequently, we verified that the power management in the case of receiving DWPT from road-side can be established by applying the proposed SOC control.

## VII. CONCLUSION

In this research, power management on the wheel-side of the advanced system of W-IWM is proposed. W-IWM2 has multiple power sources on its wheel-side, and power of these power sources are need to be managed for efficient and stable motor drive. By applying the proposed SOC control of LiC on the wheel-side, the power management can be established. Simulation and experimental results verified the establishment of the power management.



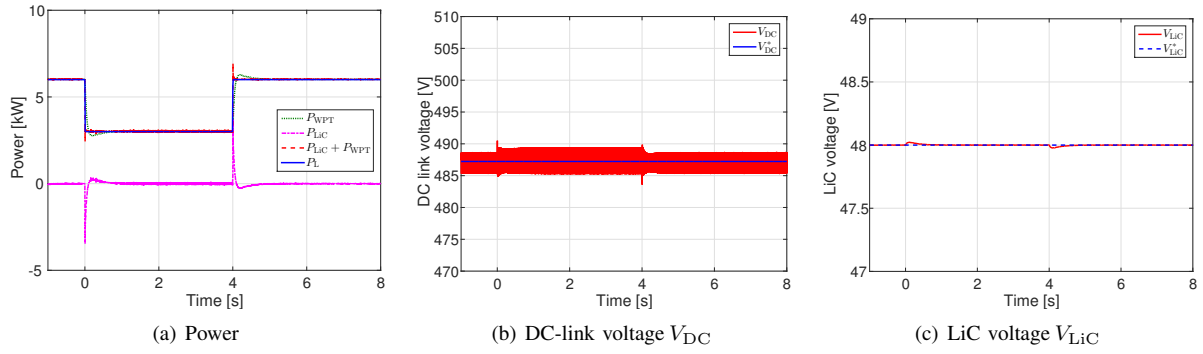


Fig. 8. Simulation results of load power increment.

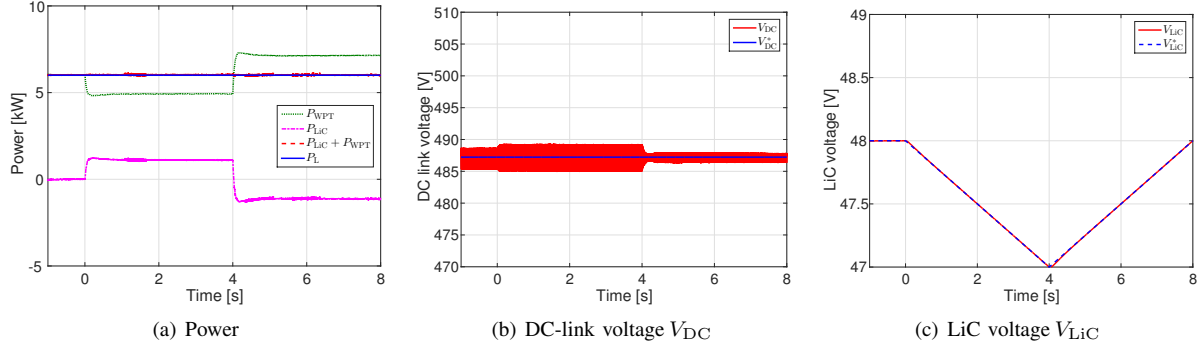


Fig. 9. Simulation results of load power decrement.

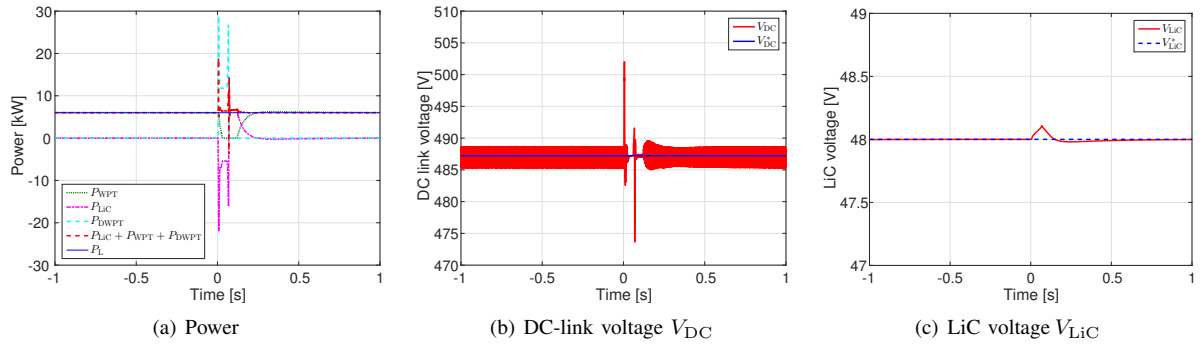


Fig. 10. Simulation results of power management with D-WPT.

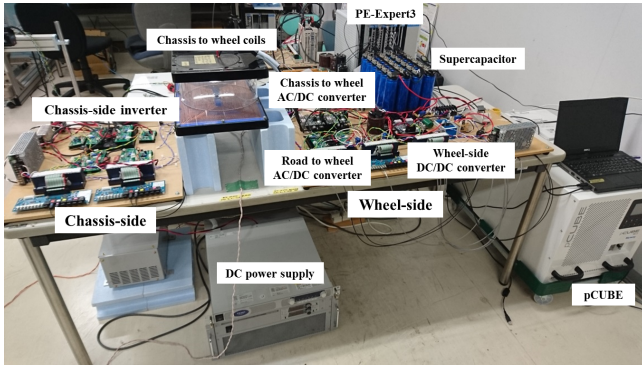
We are going to conduct large power experiment using the W-IWM2 which is under construction.

#### ACKNOWLEDGMENT

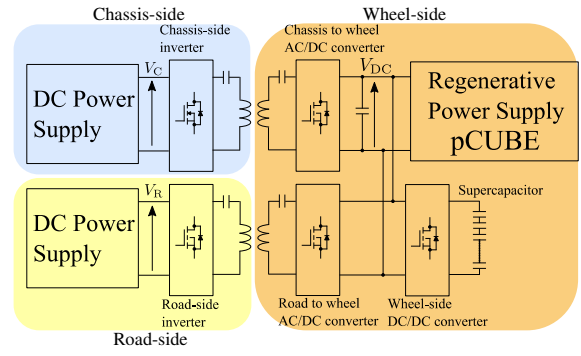
The research presented in this paper was funded in part by the Ministry of Education, Culture, Sports, Science and technology grant (No. 26249061). The authors would like to express their deepest appreciation to the Murata Manufacturing Co., Ltd. for providing the laminated ceramic capacitors (U2J characteristics) used in these experiments.

#### REFERENCES

- [1] Atsuo Kawamura, Giuseppe Guidi, Yuki Watanabe, Yukinori Tsuruta, Naoki Motoi and Tae-Woong Kim: "Driving Performance Experimental Analysis of Series Chopper Based EV Power Train", *Journal of Power Electronics*, Vol.12, No.6, pp.992–1002, (2013).
- [2] Hiroshi Fujimoto and Shingo Harada: "Model-based Range Extension Control System for Electric Vehicles with Front and Rear Driving-Braking Force Distributions", *IEEE Transaction on Industrial Electronics*, pp.3245–3254, (2015).
- [3] Yuta Ikezawa, Hiroshi Fujimoto, Yoichi Hori, Daisuke Kawano, Yuichi Goto, Misaki Tsuchimoto and Koji Sato: "Range Extension Autonomous Driving for Electric Vehicles Based on Optimal Vehicle Velocity Trajectory Generation and Front-Rear Driving-Braking Force Distribution with Time Constraint", *IEEJ Journal of Industry Applications*, Vol.5, No.3, pp.228–235, (2016).
- [4] Satoshi Murata: "Innovation by in-wheel-motor drive unit, Vehicle System Dynamics," *International journal of Vehicle Mechanics and Mobility*, Vol.50, Issue.6, pp.807–830, (2012).
- [5] Siqi Li and Chunting Chris Mi: "Wireless Power Transfer for Electric Vehicle Applications," *IEEE Journal of Emerging and Selected Topics in Power Electronics*, Vol.3, No.1, pp.4–17, (2015).
- [6] J. M. Miller, O.C. Onar and M. Chinthavali: "Primary-Side power-flow Control of Wireless Power Transfer for Electric Vehicle Charging," *IEEE Journal of Emerging and Selected Topics in Power Electronics*, Vol.3, Issue.1, pp.144–162, (2015).

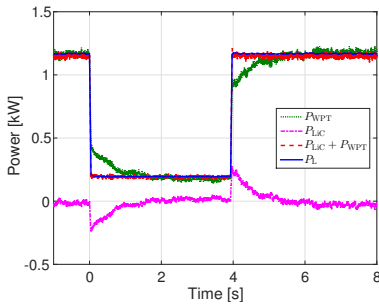


(a) Experimental setup

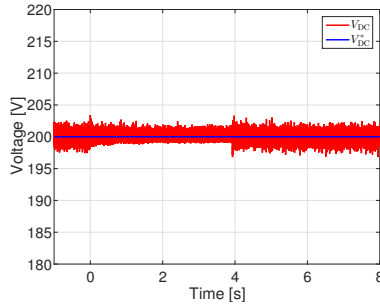


(b) Experimental circuit

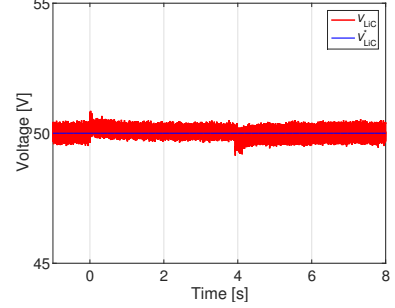
Fig. 11. Experimental setup.



(a) Power

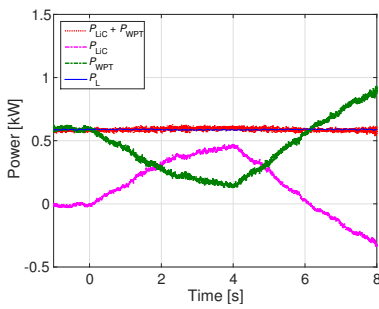


(b) DC-link voltage  $V_{DC}$

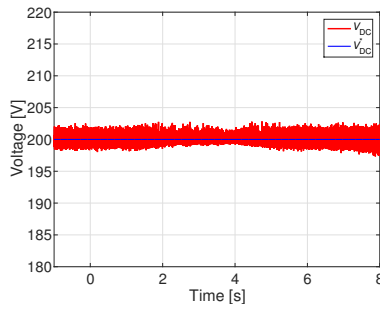


(c) LiC voltage  $V_{LiC}$

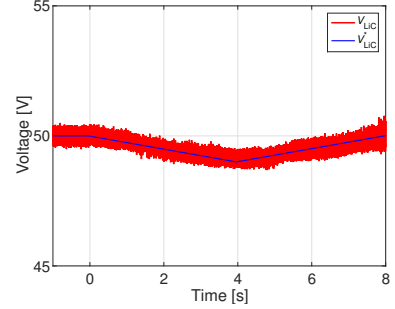
Fig. 13. Experimental results of load fluctuations.



(a) Power

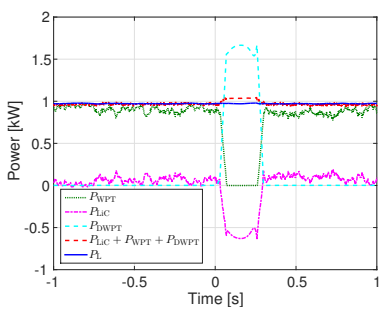


(b) DC-link voltage  $V_{DC}$

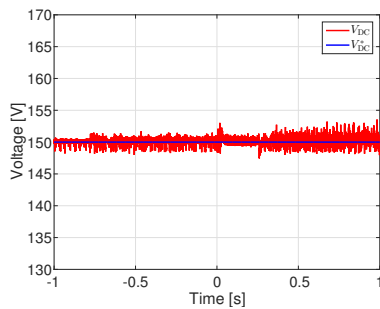


(c) LiC voltage  $V_{LiC}$

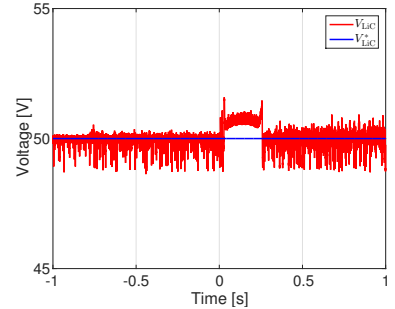
Fig. 14. Experimental results of command value changes.



(a) Power



(b) DC-link voltage  $V_{DC}$



(c) LiC voltage  $V_{LiC}$

Fig. 15. Experimental results of power management with D-WPT.

- [7] Keisuke Kusaka and Jun-ichi Itou: "Reduction of Reflected Power Loss in an AC-DC Converter for Wireless Power Transfer Systems", *IEEJ Journal of Industry Applications*, Vol.2, No.4, pp.195–203, (2013).
- [8] Motoki Sato, Gaku Yamamoto, Takehiro Imura and Hiroshi Fujimoto: "Experimental Verification of Wireless In-Wheel Motor using Magnetic Resonance Coupling", *The 9th International Conference on Power Electronics - ECCE Asia*, (2015).
- [9] Jian Cao and Ali Emadi: "A New Battery / UltraCapacitor Hybrid Energy Storage System for Electric, Hybrid and Plug-In Hybrid Electric Vehicles," *IEEE Transaction on Power Electronics*, Vol.27 No.1, pp.122–132, (2012).
- [10] Matthew McDonough: "Integration of Inductively Coupled Power Transfer and Hybrid Energy Storage System: A Multiport Power Electronics Interface for Battery-Powered Electric Vehicles," *IEEE Transaction on Power Electronics*, Vol.30, No.11, pp.6423–6433, (2015).
- [11] Daisuke Gunji, Takehiro Imura and Hiroshi Fujimoto: "Operating point Setting Method for Wireless Power Transfer with Constant Voltage Load," *41st Annual Conference of the IEEE Industrial Electronics Society*, pp.881–8856, (2015).